On the transition to chaotic scattering

1992 J. Phys. A: Math. Gen. 25 1483

(http://iopscience.iop.org/0305-4470/25/6/010)

J. Phys. A: Math. Gen. **25** (1992) 1483-1502. Printed in the UK

On the transition to chaotic scattering

R Blümel†¶, B Dietz‡, C Jung§¶ and U Smilansky‖*

† Department of Physics, University of Delaware, Newark, DE 19716, USA
‡ Department of Physics, Essen University, Essen, Federal Republic of Germany
§ Department of Physics, Bremen University, Bremen, Federal Republic of Germany
‖ H H Wills Physics Laboratory, Royal Fort, Tyndall Avenue, Bristol BS8 1TL, UK

Received 1 November 1991

Abstract. A classical scattering system is chaotic if it possesses a fractal set of trapped unstable orbits, resulting in singular deflection functions. A scattering system is regular if it supports only a countable set of trapped unstable orbits. Its deflection functions are piecewise smooth with at most a countable number of scattering singularities caused by the trapped orbits. Despite the simple structure of the deflection functions, the Poincaré scattering mapping (PSM) may be regular, hyperbolic or display mixed dynamics. Thus, the degree of chaoticity of the PSM serves as a finer scale for the discussion of the transition to chaotic scattering in the classical domain. In the quantum domain we show that the properties of the PSM determine the statistics of the eigenphases of the S-matrix, and that, if the PSM is hyperbolic, the eigenphases follow the statistics predicted by random matrix theory.

1. Introduction

The interest in chaotic scattering, and the recognition of its relevance in various fields of physics, has resulted in an ever-growing number of studies of this phenomenon. In particular, the identification of universal features which can clearly distinguish between chaotic and regular scattering is a key issue in recent research. A classical scattering system is chaotic when it possesses a non-trivial set of unstable *trapped* orbits. The properties (such as, for example, the Lyapunov exponent or the topological entropy) of this set determine the quantities which characterize the scattering process. In particular, the stable and unstable manifolds of the trapped periodic orbits extend to the asymptotic domain, resulting in classical deflection functions which are fractal functions with self-similar structures on all scales and abundant (Cantor set) singularities [1, 2].

The quantal behaviour of classically chaotic systems was shown to display universal features. The scattering matrix corresponding to such processes in the limit of small $\hbar$ fluctuates according to the prediction of random matrix theory (RMT) [3]. Another important feature which characterizes quantum chaotic scattering is the distribution of the poles of the S-matrix in the complex energy plane. It was shown rigorously [4] and semiclassically [5] that, for some typical scattering problems, there exists a lower bound to the width of the resonances, in other words poles are excluded from the strip $0 > \Im(\varepsilon_j) > -\Gamma_B$, where ε_j is the pole position in the complex energy plane, and Γ_B is the gap parameter which can be expressed in terms of the parameters of the classical

¶ Heisenberg fellow of the Deutsche Forschungsgemeinschaft.
* On sabbatical leave from the Weizmann Institute of Science.

0305-4470/92/061483+20$04.50

set of trapped orbits. In the semiclassical limit, one can show that the spacings between adjacent resonances are smaller than the typical resonance width. Thus, the semiclassical regime is the regime of overlapping resonances. The fluctuations in the observed scattering amplitudes can be attributed to the interfering contributions from a large number of poles [6, 7].

All the scattering systems which do not show chaotic scattering in the sense described above can be classified as 'regular'. Within this broad class of systems one can distinguish an interesting and important evolution of the degree of complexity of the scattering dynamics, and in the present paper we would like to discuss this issue from both the classical and the quantum mechanical points of view.

The simplest systems are those which are 'completely integrable'. We shall define the precise meaning of this concept in section 2. A typical case is the elastic scattering by a potential with spherical or cylindrical symmetry, where the angular momentum perpendicular to the scattering plane is a proper integral of the motion. More complex but still regular scattering systems are those which do not possess such integrals of motion, but, on the other hand, cannot support trapped orbits, or, at most, have a finite number of them. An example of such a system is the scattering from a convex (but not symmetric) obstacle. If such an obstacle is deformed to become concave, it can trap more and more trajectories and finally may show chaotic scattering when the set of unstable trapped orbits becomes a fractal set. In this case it is also possible to get regions of positive measure of trapped orbits.

There exist in the literature some studies of the transition of the type described above [8, 9]. In particular, interesting results were derived on the mechanism by which the number of trapped periodic orbits increases when a control parameter is varied, and the corresponding modification of the symbolic dynamics used to describe the trapped orbits. A corresponding study in the quantum domain does not exist, and in the present paper we would like to contribute towards a better understanding of the transition as observed in the quantum theory.

In our approach it is useful to consider the scattering process as a means to induce a mapping by which the parameters which define the incoming particles or wavefront are mapped into parameters which specify the outgoing particles (or waves). In wave mechanics the operator which generates this mapping is the S-matrix. In classical mechanics it is the Poincaré scattering mapping (PSM) [10], which is the classical analogue of the S-matrix. We shall devote section 2 to the definition and discussion of the PSM. Here, we shall illustrate it by means of an example: consider elastic scattering in the plane from a potential which is not cylindrically symmetric. The asymptotic parameters are the incident angle θ and the incident angular momentum l. After the scattering, the particle leaves the interaction region with the angle θ' and angular momentum l'. The primed quantities are functions of the unprimed quantities, and these functions constitute a mapping (the PSM) in the (θ, l) plane which can be shown to be area preserving. A successive application of the PSM can be understood as subjecting the particle to another scattering, in which the previous final conditions serve as initial conditions.

The PSM for a completely regular system conserves the integrals of the motion. Hence, a trace of a 'trajectory' obtained by successive applications of the PSM will occupy a torus, which, for two-dimensional problems, consists of a closed line in the (θ, l) plane. In the example mentioned above, consider the scattering from a potential with cylindrical symmetry. The integral of the motion is the angular momentum and the PSM is reduced to a twist.

At the other extreme, where chaotic scattering prevails, the functions which define the mapping are fractal functions of the type discussed above. Iterating such a mapping and plotting the results in the plane of final asymptotic variables one gets a distribution which covers evenly the entire available domain.

For scattering systems which fall between the two extremes, the mapping functions are smooth or at most display a finite number of singularities. The singularities are due to the intersection of the stable manifolds of the trapped unstable orbits with the asymptotic domain. There is a finite number of such points in systems which we consider here. In spite of the well-behaved dependence of the mapping functions on the arguments, their iterations may lead to a large variety of behaviours, ranging from regular to chaotic. Thus, the PSM provides us with a means to establish a hierarchy of complexity within the class of non-chaotic scattering systems, according to the chaoticity of the PSM. A more detailed discussion of this classification will be deferred to the next section.

Having established the hierarchy of complexity in regular scattering systems, we shall focus our attention on systems which do not display chaotic scattering, but whose PSM is hyperbolic. We shall study their classical behaviour and then quantize them and check to what extent their S-matrices follow the rules prescribed by RMT. We shall study the distribution of the eigenvalues (eigenphases) and of the matrix elements themselves. We shall show that, for this class of problems, the eigenvalue distributions follow the predictions of RMT. This behaviour is consistent with the semiclassical arguments [3] which show that the spectral two-point correlation function reproduces the RMT behaviour if the PSM is hyperbolic. The distribution of the S-matrix elements and their correlations do not necessarily follow the RMT statistics, and we show the results of an analysis of two systems. Both systems have hyperbolic PSMs (in spite of showing regular classical scattering). Their spectral distributions follow RMT, but for one of them the S-matrix statistics follow the RMT distributions, whereas for the other system there are marked deviations.

A paradigm example is the scattering from the outside of a convex billiard, which will be discussed in section 3. This scattering system is regular since there exist no trapped orbits. We shall show, however, that the PSM is completely equivalent to the mapping that describes the motion inside the billiard, and, therefore, for a proper choice of the billiard shape (e.g. stadium) it is hyperbolic. We shall then give a semiclassical argument which connects the statistics of the S-matrix of the scattering problem to the energy spectrum of the inside problem. The methods used in section 3 were first developed [11] for the purpose of semiclassical quantization of chaotic billiards from a scattering point of view. We repeat some of their derivations for the sake of completeness.

In section 4 we shall proceed with the numerical examples where we carried out detailed statistical studies of the S-matrix. Both systems are closely related to the problem of scattering from billiards, and the numerical analysis supports strongly the semiclassical ideas put forward in section 3. We shall finally summarize and discuss our findings in section 5.

2. The Poincaré scattering mapping

Assume that scattering trajectories in both the incoming and outgoing directions are labelled by the numerical values a_i of a set of phase space functions A_i which are

constants of the motion in the asymptotic domain. The Hamiltonian can be taken as one of the A_i with the corresponding value of the energy E as one of the a_i. Generic scattering trajectories possess both incoming and outgoing asymptotes, which are labelled by a_i and a_i', respectively. Thus, the set of all scattering trajectories defines a scattering mapping $\tilde{M}$ by

$$\boldsymbol{a}' = \tilde{M}(\boldsymbol{a}) \tag{2.1}$$

where $\boldsymbol{a}$ stands for the vector of asymptotic labels a_i. It should be noted that $\tilde{M}$ may be singular on a subset of measure zero in the domain of initial conditions.

The mapping $\tilde{M}$ is not yet the classical analogue of the quantum S-matrix, since S is defined relative to the free motion, whose effects are 'divided out' (using, for example, the interaction representation). In the classical domain a similar procedure is also required. In typical scattering problems A_i functions which correspond to *action* variables are constant in the asymptotic domain. The conjugate *angle* variables, however, may change periodically with time, and what remains constant are the reduced angles or the phaseshifts which survive after the free propagation in the asymptotic region is subtracted. These phaseshifts are the variables a_i which, together with the actions, specify the classical asymptotes. A problem which is intimately connected with the procedure for determining the reduced angles relates to the problem of multiple applications of the mapping $\tilde{M}$. In other words, we have to provide a mechanism by which outgoing conditions can serve as incoming conditions for the next application of the mapping.

For systems where the full Hamiltonian H can be decomposed into a free part H_0 and an interaction V, the reinjection and removal of the trivial time variation due to the free motion can be achieved in the following way. A scattering trajectory develops forward in time with the full Hamiltonian H as the generator of the motion. Once the asymptotic region (where V vanishes) is reached, we use H_0 as the generator of the motion, and run it backwards in time until the incoming asymptotic domain is reached. At this point H replaces H_0 and the time runs forward, starting a new iteration of the mapping. This successive application of the mapping $\tilde{M}$ and the reinjection mechanism described above completes the construction of the PSM.

With this picture in mind, it is clear that the PSM is completely integrable under the following conditions only. There must exist a complete set of phase space functions $\boldsymbol{K}$ which are conserved under the action of H. In addition, if we denote by $\boldsymbol{K}_0$ the functions to which $\boldsymbol{K}$ reduces in the asymptotic limit, then we require that $\boldsymbol{K}_0$ should be conserved under the action of H_0. Such a situation is as rare as complete integrability for bounded systems, and these form the class of systems to which we referred in the opening remarks as being completely integrable. The preceding analysis implies that the integrability of the Hamiltonian system does not necessarily lead to the integrability of the PSM. The situation where the Hamiltonian is integrable but the PSM is not is of particular interest for us in the present paper. The integrability of H implies that the phase space can be foliated in an invariant way by the transport of the asymptotic conditions. This, however, does not imply that the PSM is integrable. We illustrate this important observation with the following example.

Consider the scattering of a charged particle off an electric dipole in a plane. In polar coordinates:

$$H = \frac{p_r^2}{2} + \frac{L^2}{2r^2} + \frac{\cos\phi + c}{2r^2}. \tag{2.2}$$

We added a term $c/2r^2$ with $c>1$ to avoid an infinitely deep attractive potential. In this system, $K=L^2+\cos\phi+c$ is a conserved quantity. Since K is independent of r, it retains its form in the asymptotic regime, hence $K_0=K$. However, K_0 is not conserved under the action of H_0, which is here the kinetic energy part of H. Thus, the reinjection process does not conserve the value of K. This can be easily understood by actually performing the reinjection as explained above. Take an asymptote labelled by (E, L, ϕ). Reverse the time and let the particle run backwards in time with H_0 as the generator of the motion. It runs along a straight line and ends up in an asymptote which is characterized by $(E, L, \phi+\pi)$. However, for most ϕ-values, $K(E, L, \phi)\neq K(E, L, \pi+\phi)$. Besides K there is no other constant of the motion, and we therefore conclude that the PSM is not integrable, even though the Hamiltonian is analytically integrable.

The above discussion allows us to divide the set of scattering systems into three classes:

Class I—systems displaying chaotic scattering. The PSM is singular on a fractal set, there is no invariant foliation of phase space and the PSM is automatically chaotic.

Class II—systems with deflection functions with at most a finite number of singularities. Phase space might be foliated into invariant leaves by the transport of initial conditions, but the resulting PSM is chaotic.

Class III—systems for which the PSM is completely integrable. In this case a foliation of the phase space exists by the transport of the asymptotic foliation provided by the PSM. The deflection function cannot be chaotic in this case.

Class III systems are the scattering analogues of integrable bounded systems. They are structurally unstable against weak perturbations. Systems in class II or in class I can be structurally stable. Class II systems provide a type of integrability of the Hamiltonian dynamics in phase space which can be stable in contrast to the integrability of bounded systems. The PSM for systems in class II can be either completely hyperbolic, or may show the interwoven structures of elliptic islands within hyperbolic stripes. In the next sections we shall study systems which belong to class II and whose PSM may show the features mentioned above.

3. Scattering from convex billiards

As a first example of class II systems, consider elastic scattering from a convex billiard in the plane. Classical trajectories are determined by specular reflections, and the corresponding wave-scattering problem has to be solved with Dirichlet boundary conditions.

Classical scattering from the convex billiard is definitely not chaotic: there exist no trapped orbits, and the classical deflection function is continuous as long as the billiard has a boundary with a continuous derivative (this will be assumed throughout). The asymptotic phase space is a cylinder which is defined in terms of the incidence angle θ and the angular momentum l, which we shall express in units of $\hbar$. The angular momentum is defined relative to a reference point inside the billiard. For any given θ there exist two limiting values of the angular momentum, $l_-(\theta)$ and $l_+(\theta)$ such that no reflection occurs for trajectories which aim at the billiard at an angle θ with $l<l_-(\theta)$ or $l>l_+(\theta)$. An intermediate value $l_b(\theta)$ can also be defined as the angular momentum at which the deflection is exactly backwards. The deflection function $\Theta(l;\theta)$ for a given θ has a single maximum $\Theta=\pi$ at l_b. The lines $l_+(\theta)$ and $l_-(\theta)$ determine a stripe

Σ on the cylinder. Points outside Σ are not affected by the billiard and hence they are mapped onto themselves by the scattering process. A point (θ, l) in Σ is mapped by the scattering into (θ', l') which is also in Σ. Thus, Σ is the domain of the PSM.

The PSM in the present case is constructed in the following way. A point $(\theta, l) \in \Sigma$ corresponds to a straight line trajectory which is incident on the billiard at an angle θ and an impact parameter $b = l/k$ with k the wavenumber (see figure 1). The trajectory scatters into the direction θ' with an angular momentum l' and the corresponding impact parameter b'. The next application of the PSM is realized by considering (θ', l') as defining an incoming trajectory. It moves on the same line as the previous outgoing trajectory, but it impinges on the scattering at a diametrically opposite point. The generating function which induces the mapping is given in terms of the reduced action

$$\Phi = -\left(\int r \, dp_r + \int \theta \, dl\right) \tag{3.1}$$

where r and p_r are the distance from the reference point and the conjugate momentum, respectively. One can easily show that Φ is a sum of two terms, and each corresponds to (minus) the integral of the radial momentum from the point of least approach on the incoming or outgoing branch of the trajectory to the point of impact on the billiard. (In other words Φ is the sum of the WKB phaseshifts incurred in the incoming and outgoing branches of the trajectory. The phaseshift is negative due to the repulsive scattering potential.)

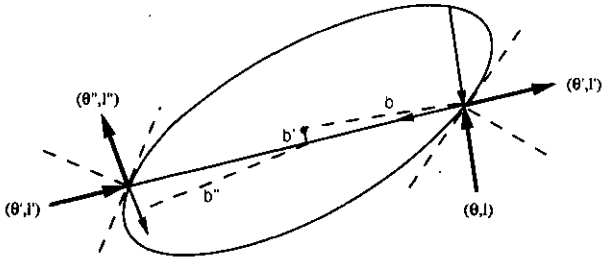

Figure 1. Bounded trajectories of a particle that is trapped inside a convex billiard and trajectories of particles which are scattered from it.

Any external scattering $(\theta, l) \rightarrow (\theta', l')$ corresponds to an internal trajectory which impinges on the billiard at the same point with opposite incoming and outgoing directions and the same values of the angular momenta but for a change of sign (see figure 1). Since the dynamics inside the billiard is completely described as a two-dimensional mapping (here we use the (θ, l) representation), the correspondence between the scattering dynamics and the internal dynamics is established. The action $-\Phi$ (see (3.1)) serves also as the generating function for the internal mapping.

It should be noted that the requirement that the billiard is convex (rather, non-concave) was essential for the previous discussion. The PSM involves scattering trajectories which impinge only once on the billiard, which is the basic ingredient in establishing the one-to-one correspondence between the PSM and the internal mapping. It allows the use of the polar coordinates to describe the dynamics, instead of the more generally applicable representation in terms of the arc length and the impact direction. Finally, it eliminates the occurrence of 'ghost' trajectories (see [12, 13]). The one-to-one correspondence between the dynamics induced by the PSM on Σ, and the

classical dynamics of a particle which is trapped *inside* the billiard has very important consequences. The shape of the billiard determines the degree of chaoticity of the dynamics inside (e.g. see [14, 15]). Hence the conjugate PSM can display any degree of chaoticity when considered as a mapping on Σ, even though the underlying scattering process itself is not chaotic.

We return now to the quantum domain, where we would like to show that there exists a profound connection between the energy spectrum of the quantized motion inside the billiard and the spectrum of the eigenphases of the scattering matrix for the 'outside' problem. We shall start by deriving a semiclassical secular equation, which is written in terms of the S-matrix, and whose zeros are the eigenenergies of the quantized 'inside' problem.

A general scattering wavefunction which vanishes on the billiard boundary can be written for $\boldsymbol{r}$ outside the billiard as

$$\Psi_l(\boldsymbol{r}) = H_l^-(\boldsymbol{r}) + \sum_m \tilde{S}_{l,m} H_m^+(\boldsymbol{r}) \tag{3.2}$$

where $H_l^{\pm}(\boldsymbol{r})$ are incoming and outgoing cylindrical waves with angular momentum l. $\tilde{S}$ is the scattering matrix.

$\Psi^{(I)}(\boldsymbol{r})$ as defined above is also a solution of the Schrödinger equation inside the billiard, and it satisfies the boundary conditions on the billiard boundaries, but in general it does not represent a bound state because it is not necessarily regular at the origin. A linear combination of $\Psi^{(I)}(\boldsymbol{r})$ would represent a bound state if the irregular radial parts all appear with vanishing coefficients. The condition for this to happen is

$$Z(E) = \det(I - \tilde{S}(E)) = 0 \tag{3.3}$$

which is the desired secular equation for the 'inside' quantized billiard. The matrix $\tilde{S}$ is of infinite dimension. This is why $Z(E)$ as expressed above is not very useful. If we define $L_- = \min(l_-(\theta))$ and $L_+ = \max(l_+(\theta))$ then, for any l which is sufficiently far from the interval (L_-, L_+), and for any m, we have

$$\tilde{S}_{l,m} \approx \delta_{l,m}. \tag{3.4}$$

This means that the value of the determinant (3.3) is always vanishingly small and, in order to extract useful information, a way to discard the contribution from the physically uninteresting domain should be found. This is naturally achieved in the semiclassical domain, since here the approximate form (3.4) becomes progressively more exact. Thus we can truncate $\tilde{S}$ to the domain

$$L_- \leq l \qquad m \leq L_+ \tag{3.5}$$

and replace (3.3) by a semiclassical secular equation

$$Z_{sc}(E) = \det(I - S(E)) = 0 \tag{3.6}$$

where S is a matrix of dimension $L = L_+ - L_-$ which is obtained by restricting $\tilde{S}$ to the domain (3.5), and which is semiclassically unitary, due to (3.4).

To establish a correspondence between the energy spectrum of the billiard and the eigenphase spectrum of the S-matrix, we use an argument which was first introduced by Bogomolny [16] and independently by Doron [17].

A zero of the secular equation occurs each time that any of the eigenphases of the S-matrix $\theta_l(E)$ equals an integer multiple of 2π. Hence, the spectral density $d(E)$ can

be expressed as

$$d(E)=\sum_i \delta(E-E_i)=\sum_{l=1}^{L}|\tau_l|\delta_p(\theta_l(E)) \tag{3.7}$$

where $\tau_l=\theta_l'(E)$, and the prime denotes differentiation with respect to E. $\delta_p(x)$ is the periodic δ-function. Let us consider the spectral density at an interval of size Δ about a mean energy E_0. Δ is taken to be large on the scale of the mean level separation, which is given by Weyl's formula to be $2\pi\hbar^2/A$ where A is the area enclosed by the billiard. Then, for $\varepsilon=(E-E_0)<\Delta$

$$d(\varepsilon)\approx\sum_{l=1}^{L}|\tau_l|\delta_p(\theta_l(E_0)+\varepsilon\tau_l). \tag{3.8}$$

The τ_l are proportional to the eigenvalues of the time delay matrix $1/i[S'S^\dagger]$, and therefore their distribution reflects the distribution of time delays in the classical scattering process. (Note that the τ_l have the dimension of inverse energy.) In the present case of scattering from convex billiards, all the delay times are negative. Denote by τ the mean delay time. If we were able to show that the fluctuations in the distribution of the τ_l about their mean τ are small, we could replace all the τ_l in (3.8) by τ. Defining $\theta=\varepsilon|\tau|$ we would get

$$d(\varepsilon)\approx|\tau|\sum_{l=1}^{L}\delta_p(\theta_l(E_0)-\theta) \tag{3.9}$$

which would have established the correspondence between the energy spectral density (the LHS of (3.9)) and the eigenphase spectral density (the RHS of (3.9)). Equation (3.8) is an approximation which holds only in the vicinity of the mean energy E_0. The values of the eigenenergies derived from the higher values of the angular momentum l are not expected to be accurate, because they are the waves for which the approximation (3.4) is expected to be at its worst. If we exclude the extreme values of l, and if the billiard is not too deformed, the classical delay time distribution will depend only slightly on the impact parameter and angle of incidence, and hence the corresponding τ_l distribution is expected to be well centred about its mean value. This point is a central issue in [18], where it is shown that, in the semiclassical limit, the width of the τ_l distribution decreases as $\hbar$ approaches zero.

Assuming the approximate validity of (3.9) we can come to the following conclusion. Take a billiard whose 'inside' problem displays classical chaos and therefore its energy spectrum can be described statistically in terms of random matrix theory. Then, the spectral statistics of the S-matrix eigenphases follows the same statistics even though the corresponding scattering is not chaotic. This argument is consistent with the observation mentioned above that the semiclassical proof [3] that the eigenphases spectrum follows RMT requires only that the PSM be chaotic when iterated as a mapping. If, on the other hand, the 'inside' problem is integrable and the energy spectrum is Poissonian, one would expect the same for the eigenphases spectrum of the corresponding S-matrix.

4. Examples

In the present section we shall illustrate the results obtained above by presenting a numerical solution of two scattering problems.

4.1. The 'frying pan'

The scattering occurs inside a domain which consists of a part of a circle which is joined to an infinitely long channel (see figure 2). According to a theorem introduced in [14], the motion in the billiard, which is obtained by closing the circular part along the chord that is common to the circle and the channel, is chaotic. A particle is injected along the channel and, after a few reflections in the circular part, it emerges again in the channel. The asymptotic region in the present system is the channel where the motion is separable in rectangular coordinates. We shall denote by (x, y) the longitudinal and transverse coordinates, respectively. The y-axis coincides with the chord which is common to the circle and the channel, and the x-axis runs at the centre of the channel. We measure distances in units of the radius of the circle, and denote by d the distance of the channel from the centre of the circle. W denotes half the channel width.

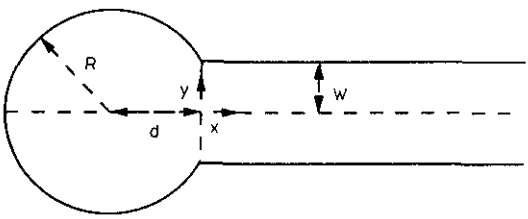

Figure 2. Sketch of the 'frying pan'. A particle is injected along the channel and after a few reflections in the circular part it is scattered back into the channel.

The y-motion inside the channel is bounded and can be treated as an internal degree of freedom, for which action angle variables are the most appropriate coordinates. The action is just the absolute value of the y-momentum,

$$I = |p_y|. \tag{4.1}$$

The total energy E and I will be used as the first two asymptotic labels of scattering trajectories. The corresponding angle variable is

$$\phi = \pi\left(\frac{W+y}{2W}\Theta(p_y) + \frac{3W-y}{2W}\Theta(-p_y)\right) \tag{4.2}$$

where $\Theta(x)$ is the unit step function. ϕ is an example of an angle variable which is changing periodically along the asymptotic trajectory. Its reduced value is

$$\tilde{\phi} = \phi - \pi\frac{Ix}{2Wp_x} \tag{4.3}$$

and a direct computation shows that $\tilde{\phi}$ is constant along the trajectory. Besides the variables E and I it can therefore be used as a third label to specify a scattering asymptote. From now on we shall not consider the trivial energy dependence of the problem, and consider the scattering as a mapping of the $(I, \tilde{\phi})$ space onto itself. Note that the constant energy condition implies that this space is bounded: $I \leqslant (2E)^{1/2}$.

In a typical scattering experiment, the incoming energy and action variables are well defined, but the initial phase angle is not, resulting in a distribution of final outgoing momenta. The function $I_{\text{out}}(\tilde{\phi}_{\text{in}})$ plays here the role of a deflection function. Since the motion inside the circular region is regular there exist no unstable trapped

orbits and our system does not show topological chaos. The deflection function has only a finite number of singularities for typical values of I_{in}. There exist exceptional values of I_{in} for which there might be an infinite number of singularities which have only a finite number of accumulation points. This is clear evidence for the absence of chaotic scattering in this problem. Figure 3 shows a typical deflection function.

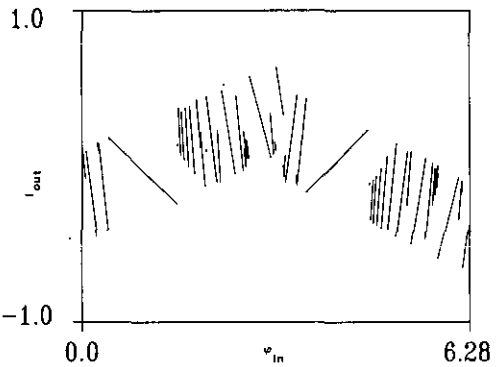

Figure 3. The deflection function $I_{out}(\tilde{\Phi}_{in})$ for fixed $I_{in} = 0.1$ and parameter value $d = 0.95$.

Another way to show that the present system is not chaotic is by considering the delay time, i.e. the time spent by the particle inside the circular region. Assume that the particle crosses the y-axis at a given angle and y-coordinate. These values define the angular momentum which labels the torus on which the particle moves when it scatters off the circle. The smaller W the longer (on average) will be the time which the particle spends inside, but eventually it will leave after a finite time. The existence of a maximal number $N_{max}(I)$ of bounces off the circle for any value of I is another indication of the lack of chaotic scattering in the present system.

To define the PSM we chose as a reference system the free motion in the channel $x > 0$, $|y| < W$. This choice of the free Hamiltonian gives a reinjection mechanism which implies that

$$(\tilde{\phi}, I)_{in} = (\tilde{\phi}, I)_{out}.$$

Hence, successive applications of the PSM can be visualized by positioning a straight reflector on the chord at $x = 0$. The dynamics described by the PSM is thus the dynamics inside a *closed* billiard where one constructs a Poincaré mapping by considering a section in phase space which consists of the straight chord at $x = 0$. The relation between the 'inside' and the 'outside' problems is of the same kind as discussed in the previous section.

The PSM is completely chaotic for any value of $0 < d < 1$. Numerical simulations show that any trajectory of the PSM covers uniformly the available phase space. In figure 4 we show the numerical values deduced for the classical Lyapunov exponent as a function of d. The PSM is integrable for $d = 0$, since the angular momentum is a conserved quantity for $d = 0$.

The quantum mechanical problem is solved by obtaining solutions of the Helmholtz equation with Dirichlet boundary conditions on the boundaries of the 'frying pan'. At any given wavenumber k, the channel can support a finite number of propagating modes, whose number is given by the integer part of Wk/π. Since the entire system is symmetric under $y \to -y$, the S-matrix is reducible, and we shall confine ourselves

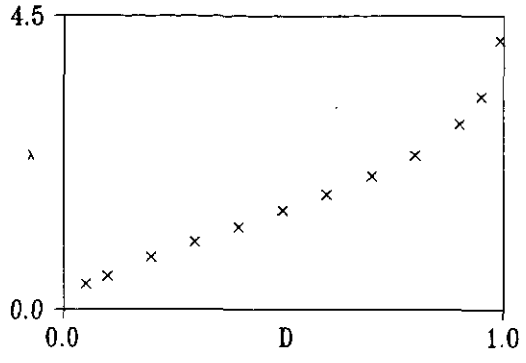

Figure 4. The Lyapunov exponent of the PSM for the frying pan as a function of d.

here to the subspace of antisymmetric wavefunctions. Scattering solutions at $x \to \infty$ can be decomposed into a linear combination of incoming and outgoing plane waves in the conducting modes. This defines the S-matrix, which, in the present case is a symmetric and unitary matrix of dimension L.

The actual numerical solution was carried out by extending the method used in [19]. Numerical difficulties arise because of the corners at the joining points of the channel to the circle [20]. We have solved them in the present case by a method which is reported in the appendix, where we also describe briefly other issues which arise in the numerical work. The reliability of the calculations was tested by checking the unitarity of the calculated S-matrix. We found that matrices of dimension $L \leq 50$ can be computed for the range $0 \leq d \leq 0.75$ with reasonable accuracy. The deviation of the absolute value of the determinant of S, $|\det S|$, from the value 1 is 10^{-4}.

To test the statistical properties of the S-matrix, we generated a database in the following way. We chose for d the values $d = 0$, 0.035, 0.05, 0.1, 0.3, 0.5 and 0.75, which allow us to scan the onset of chaoticity of the PSM in some detail. For each value of d we calculated at least 24 S-matrices with $L = 8$, 25 and 50. The S-matrices for the same d and L were calculated for k-values whose difference exceeded the k correlation length [18], thus ensuring statistical independence. Using this database we were able to compare our data with the predictions of RMT for the canonical ensemble of unitary, symmetric matrices (COE).

We first checked the distribution of eigenphases. The semiclassical theory [3] as well as the discussion in section 2 suggest that the chaoticity of the PSM is sufficient to ensure that the eigenphases distribution follows the predictions of the RMT in the semiclassical limit. We find that this is indeed the case for the two statistical tests which are commonly used in similar studies. The nearest level distribution is shown in figure 5 for $L = 50$ and various values of d. The transition between the Poisson distribution at $d = 0$ and the Wigner distribution occurs rather rapidly and already for $d \approx 0.2$ one finds a good agreement with the Wigner distribution. The Σ^2 statistics is plotted in figure 6 for the same set of S-matrices. The same trend of a transition toward the COE predictions is observed. Similar tests with matrices of lower dimensions give similar results, with the difference that the values of d where the transition to COE-like behaviour occurs is progressively higher for lower values of L. This behaviour can be understood on the following grounds [3, 21]. The inverse of the Lyapunov exponent defines a classical mixing time n_c. The semiclassical connection between classical chaoticity and the RMT statistics requires that $L \gg n_c \gg 1$. The requirement $L \gg n_c$ is

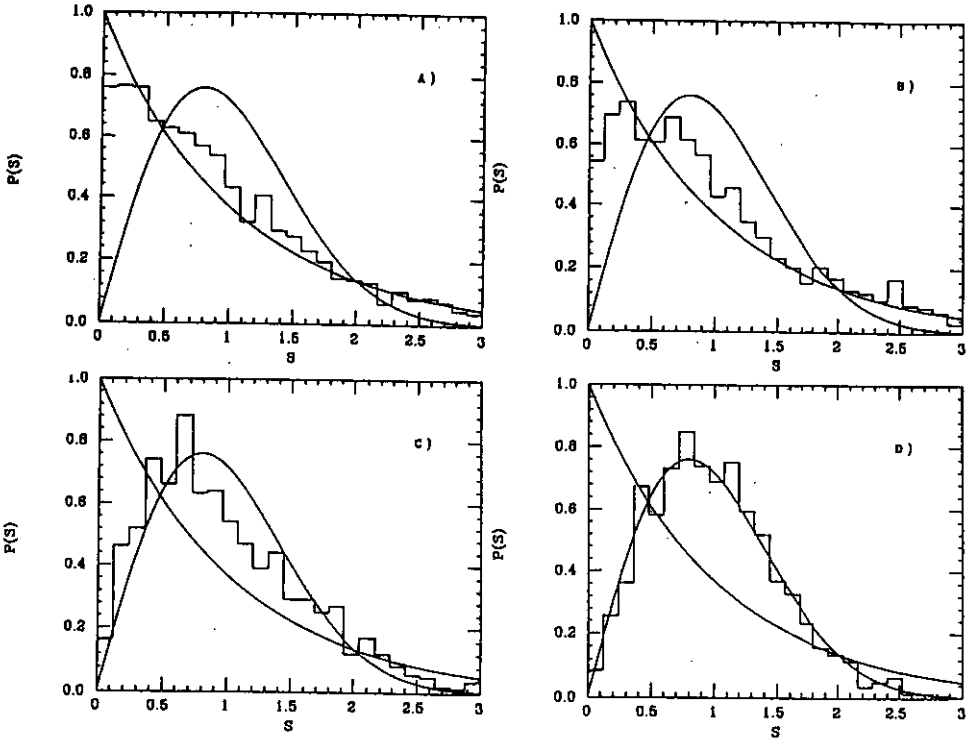

Figure 5. Nearest-neighbour spacing distribution for $L=50$ and (*a*) $d=0$, (*b*) $d=0.035$, (*c*) $d=0.1$ and (*d*) $d=0.3$. The variable S measures the spacing between two adjacent eigenphases in units of the mean spacing $2\pi/L$. The smooth curves correspond to the Poisson and Wigner distributions.

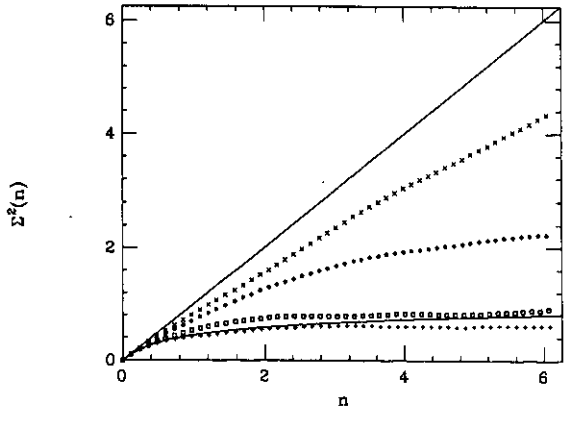

Figure 6. The Σ^2 statistics for the same values of d and L as in figure 5: $\times$, $d=0$; $\diamond$, $d=0.035$; $\square$, $d=0.1$; $+$, $d=0.3$.

easily fulfilled in the semiclassical limit since n_c is a classical timescale, whereas $L \approx 1/\hbar$. From figure 4 we learn that $n_c \approx 2$ at $d = 0.1$. We expect therefore to see deviations from the COE predictions for $d \approx 0.1$.

We now turn to tests which involve the distribution of the matrix elements of the S-matrix. The canonical COE ensemble requires that the mean value of any matrix element is zero. Thus, we have to ensure that in our system the energy-averaged S-matrix, $\langle S \rangle$, is zero. In other words we should avoid 'direct' processes, which would correspond classically to the contributions from trajectories with short delay times. We tested $L^{-1}\,\mathrm{tr}(\langle S\rangle\langle S\rangle^{\dagger})$ as a measure of the importance of the direct component as we change d. Its value varies between 0.01 and 0.035.

Semiclassical arguments [3, 18] show that the matrix elements of the S-matrix may be correlated, depending on the smoothness of the distribution of the classical angle variables of the emerging trajectories. In the present case, the distribution of $\tilde{\phi}$ is uniform for not too small d-values, and we expect that our S-matrices will behave statistically like the COE.

The first numerical check consists of the distribution of the normalized transition strengths

$$x_{i,j} = L|S_{i,j}|^2. \tag{4.4}$$

RMT predict that the non-diagonal x have an exponential distribution with unit mean, while time-reversal symmetry results in an exponential distribution for the diagonal elements which is twice broader. There is a good overall agreement between this expectation and the numerical data as is seen in figure 7. A more quantitative χ^2 fit

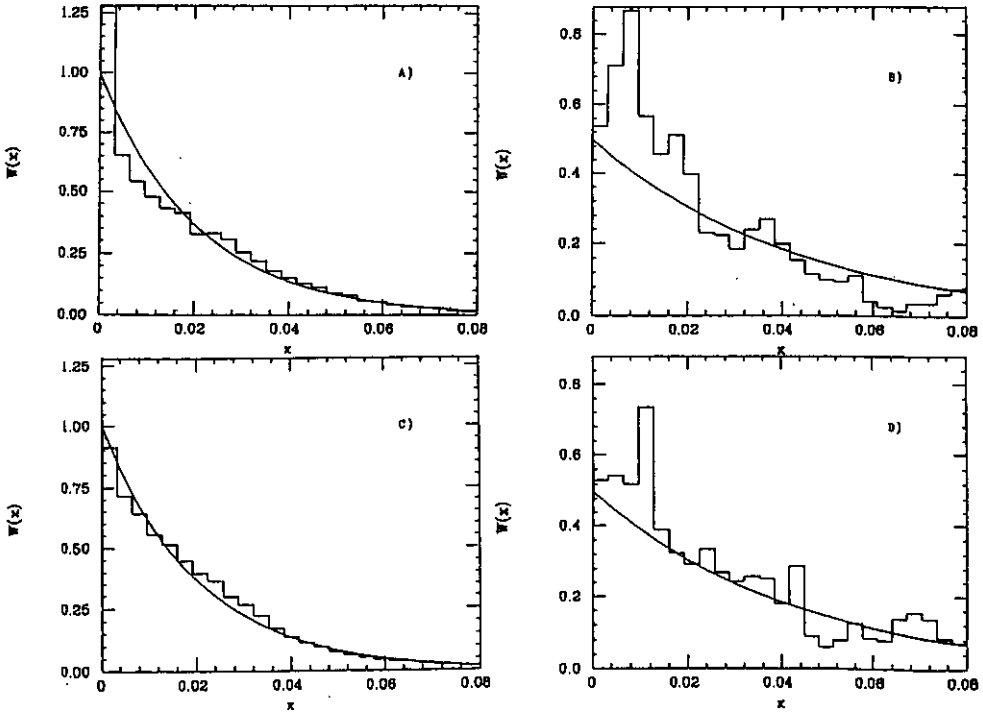

Figure 7. Distribution of the squared absolute value of the off-diagonal and the diagonal elements of S. The results for $d = 0$ are shown in (a) and (b), those for $d = 0.3$ in (c) and (d). x measures $|S_{ij}|^2$ in units of $1/L$.

of an exponential to the data showed some systematic deviation in the deduced values of the mean value and the intersection at $x = 0$.

To check correlations between S-matrix elements we calculated the correlation functions $F_{n,m}(\eta)$ defined in [3, 22]:

$$F_{n,m}(\eta) = L\left\langle \frac{1}{(2M+1)^2} \sum_{\nu=-M}^{M} \sum_{\mu=-M}^{M} S^*_{n+\nu,m+\mu} S_{n+\nu,m+\mu+\eta} \right\rangle \tag{4.5}$$

where $M \ll L$ and the triangular brackets stand for k averaging. The COE prediction for these functions is that they are Kronecker δ-functions in η. The numerical functions obtained for various d-values are shown in figure 8; the trend of getting narrower distributions as d increases is quite clear.

In summary we can say that the numerical tests performed on the present system confirm the semiclassical argument which establishes the link between COE-like behaviour of S-matrices and the chaoticity of the underlying PSM.

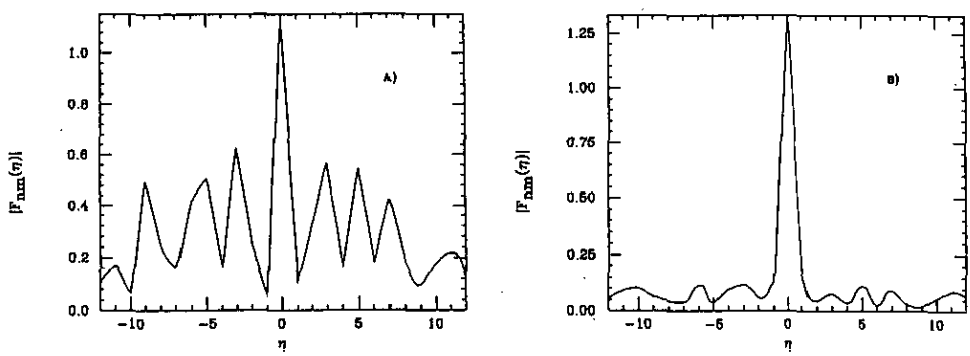

Figure 8. The absolute value of the correlation function $F_{nm}(\eta)$ for $n = 32$, $m = 27$ and $M = 7$: (*a*) $d = 0$, (*b*) $d = 0.75$.

4.2. Scattering from an array of hard discs

Consider an infinite array of identical non-overlapping hard discs equally spaced along the y-axis in the plane. Systems of this kind were studied in [23] classically and in [24] quantum mechanically. The y-momentum and the reduced y-coordinate $\tilde{y}$ serve as the action angle coordinates which label trajectories in the asymptotic domain, and the periodicity of the scatterers along the y-axis makes this coordinate a proper angle variable. In [23, 24] the scattering potentials were chosen to be attractive, and gave rise to chaotic scattering. The present example does not show classical chaotic scattering since there exists only one unstable trapped periodic orbit along the segment of the y-axis between neighbouring discs. The deflection function $p_y^{\text{out}}(\tilde{y}_{\text{in}})$ is affected by this trajectory, resulting in a strong focusing in the x-direction.

One can easily see that the PSM in this problem is equivalent to the dynamics inside a Sinai billiard, defined with periodic boundary conditions. Hence this system belongs to class II with a hyperbolic PSM.

The quantum mechanical solution of this problem was outlined in [24] and in order to apply it to the hard disc model the hard disc phaseshifts were supplied as the only necessary input. The periodicity in the y-direction implies that scattering is possible

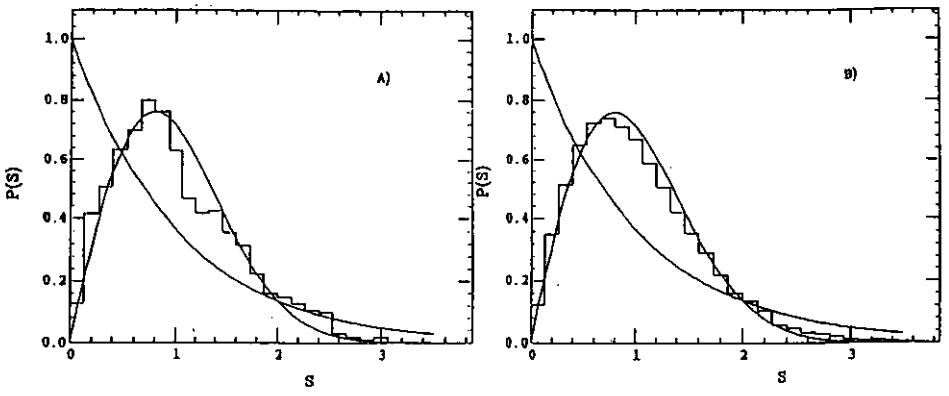

Figure 9. Nearest-neighbour spacing distribution for $L=380$ and an infinite array of identical (a) hard discs and (b) attractive scattering potentials. S measures the spacing between adjacent eigenphases in units of the mean spacing $2\pi/L$. The smooth curves correspond to the Poisson and Wigner distributions.

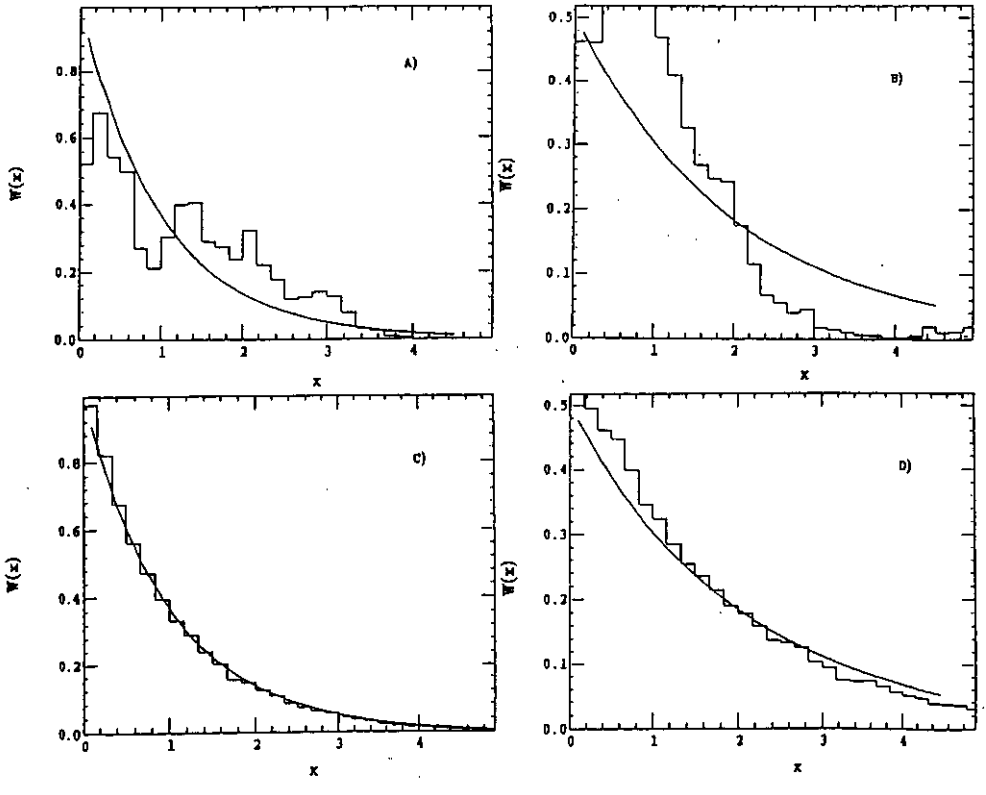

Figure 10. Distribution of the transition strength for off-diagonal and diagonal elements of S. (a) and (b) show the results for the hard disc problem, (c) and (d) those for the attractive scattering potential.

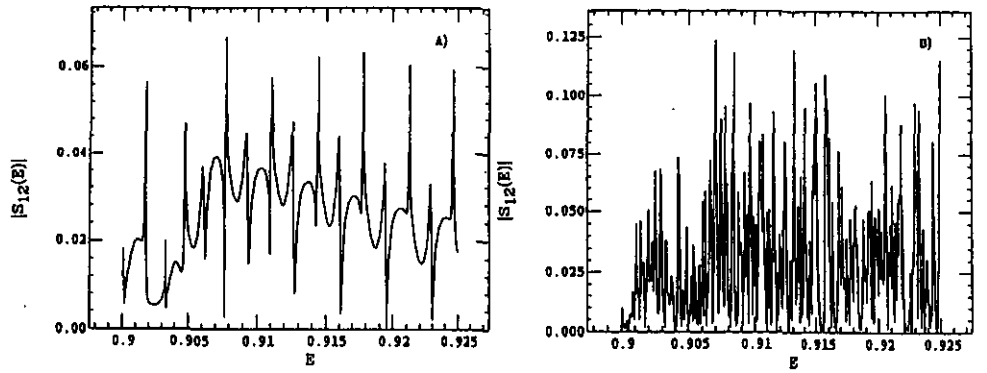

Figure 11. The dependence of $|S_{12}|^2$ on the energy in the (a) hard disc and (b) attractive scattering potential models.

only into a discrete (Bragg) manifold of directions, which are specified by the quantized values of the y-momentum. A database of S-matrices of dimension $L = 380$ was generated, and a comparison between the predictions of the COE and the results of the numerical calculations was carried out as was done for the previous example.

Figure 9 shows the nearest-neighbour distribution of the phases of the S-matrix of the hard disc model and for comparison the corresponding distribution obtained for an infinite array of attractive scattering potentials. The agreement with the Wigner function is in both cases very good. The distributions of the normalized transition elements (4.4) are presented in figure 10. For the hard disc model they show appreciable deviations from the COE predictions, which are most probably due to the strong focusing observed in the classical distribution of final directions. Figure 11 presents the typical behaviour of the absolute value of an off-diagonal element of the scattering matrix as a function of E. Resonances reappear periodically in the hard disc model and their number is small compared to that in the model with attractive scattering potential, where one finds a random behaviour of the transition strength as a function of E. Figures 10(b) and 11(b) reproduce the behaviour one generally finds for class III systems, while in class II systems the matrix elements, as one can see in figures 10(a) and 11(a), do not need to behave like that.

In summary, we may say that the numerical tests confirmed our expectations that the chaoticity of the PSM is sufficient to ensure that the S-matrix eigenphases distribute according to the COE predictions. The distribution of the matrix elements themselves may also follow the COE predictions if further conditions are met.

5. Summary

The main result of the present paper is that some of the RMT attributes of the S-matrix, in particular the distribution of its eigenphases, do not require the strong condition that the underlying classical scattering is chaotic. Rather, a much weaker requirement is sufficient, namely that the PSM taken as a mapping of the asymptotic domain onto itself is chaotic. For systems which do show classical chaotic scattering, the PSM is certainly chaotic, and therefore their quantum counterparts follow the statistics predicted by RMT to a very high accuracy.

There is a general question which is relevant to the discussion presented here and elsewhere concerning the study of the distribution of the matrix elements of the S-matrix. One could argue that the values of the S-matrix elements depend on the representation, and hence their distribution is arbitrary (within the constraint of unitarity and symmetry). The answer to this question is easy if one constructs the ensemble of S-matrices as we did in the numerical studies reported above. We constructed it by considering a family of S-matrices for a set of energy values. The spacing between successive energies is taken to exceed the energy correlation length, so that the ensemble members are uncorrelated. Non-integrability implies that there exists no *energy-independent* representation in which all the S-matrices can be diagonalized. This justifies the application of statistical methods and the relevance of statistical studies to the distribution of the matrix elements as well as the eigenvalues of the S-matrix. As a matter of fact, in a recent study [25] Doron and Smilansky showed that an ensemble of 2×2 S-matrices reproduces the *invariant measure* of the COE ensemble for $N=2$ [26]. This is the strongest possible check for the RMT and it supports the approach taken here.

Acknowledgments

US acknowledges the hospitality of Professor M V Berry and the H H Wills Physics Laboratory at the University of Bristol, where part of this research was carried out. The work was partially supported by grants from the US-Israel Binational Science Foundation (BSF) and the German Israeli Foundation for Scientific Research and Development (GIF). RB and CJ are grateful for financial support by the Deutsche Forschungsgemeinschaft.

Appendix 1. Quantum mechanical evaluation of the scattering inside the 'frying pan'

The Schrödinger equation for this problem corresponds to that of a free particle with Dirichlet condition on the boundary of the 'frying pan'. Since the entire system is symmetric under $y\to -y$ we shall confine ourselves to the upper half of the frying pan and will consider only the antisymmetric wavefunctions.

In the channel region the Schrödinger equation reads

$$-\left(\frac{\partial^2}{\partial x^2}+\frac{\partial^2}{\partial y^2}\right)\Psi_{\rm ch}(x,y)=k^2\Psi_{\rm ch}(x,y) \qquad x\in[0,\infty] \qquad y\in[0,W] \tag{A.1}$$

and the boundary conditions are

$$\Psi_{\rm ch}(x,W)=0 \qquad \forall x. \tag{A.2}$$

With

$$k^2=k_r^2+\left(\frac{\pi r}{W}\right)^2 \tag{A.3}$$

the scattering solution is given by

$$(\Psi_{\rm ch}(x,y))_r=\left\{\frac{1}{\sqrt{|k_r|}}\,{\rm e}^{-{\rm i}k_r x}\frac{1}{\sqrt{W}}\sin\left(\frac{\pi r}{W}y\right)+\sum_{t=1}^{L+M_{\rm C}}T_{rt}\frac{{\rm e}^{{\rm i}k_t x}}{\sqrt{|k_t|}}\frac{1}{\sqrt{W}}\sin\left(\frac{\pi t}{W}y\right)\right\} \tag{A.4}$$

where the first term in the braces corresponds to an incoming propagating mode, while in the second term the sum is taken over all outcoming propagating and a finite number of decaying modes. For propagating modes

$$k_r^2 = k^2 - \left(\frac{\pi r}{W}\right)^2 \geq 0. \tag{A.5}$$

Hence, their number L is given by the integer part of Wk/π. k_t is complex if $t \geq L$, yielding an exponentially decaying contribution to the sum in (A.4). We take into account only a finite number M_C of these closed channels so that (T_{ij}) is a $L \times (L + M_C)$ matrix. The reduced T-matrix with $i, j \leq L$ provides the $L \times L$ scattering matrix.

In the circular part of the 'frying pan' the Schrödinger equation reads

$$-\left(\frac{\partial^2}{\partial r^2} + \frac{1}{r}\frac{\partial}{\partial r} + \frac{1}{r^2}\frac{\partial^2}{\partial \varphi^2}\right)\Psi_{ci}(r, \varphi) = k^2 \Psi_{ci}(r, \varphi) \qquad r \in [0, R] \qquad \varphi \in [\alpha, \pi] \tag{A.6}$$

with

$$\alpha = \tan^{-1}\left(\frac{W}{d}\right) \qquad R^2 = d^2 + W^2.$$

$\Psi_{ch}(r, \varphi)$ has to fulfil the boundary condition

$$\Psi_{ci}(R, \varphi) = 0 \qquad \forall \varphi. \tag{A.7}$$

The solution of the Schrödinger equation is given as a linear combination of products of sine and spherical Bessel functions,

$$\Psi_{ci}(r, \varphi) = \sum_{m=1}^{\infty} a_m \sin(m\varphi) J_m(kr) \tag{A.8}$$

which is truncated in numerical simulations at $m = M_G$. This ansatz has to be inserted into (A.7) in order to obtain the coefficients a_m. There are several possibilities to take into account the boundary condition. One can choose a set of discrete points along the circular boundary and require that $\Psi_{ci}(R, \varphi)$ vanishes for the corresponding values of φ. In order to keep the remaining flux through the boundary negligibly small the number of these points has to be comparably high. A much more efficient method is to expand $\Psi_{ci}(R, \varphi)$ in a complete set of suitably chosen orthogonal polynomials defined in $[\alpha, \pi]$ and to require that the expansion coefficients vanish.

For both methods numerical difficulties arise from the corners where the circular and the channel part are connected. To overcome them one has to choose a very high density of points around the corners when applying the first method, which thus turns out to be very costly and inefficient. For the second method an appropriate choice are the Chebychev polynomials $T_j(x)$, $x \in [-1, 1]$, since they have a weight function $\omega(x) = 1/\sqrt{1-x^2}$, which is maximal at the borders of the range of x,

$$\int_{-1}^{1} \mathrm{d}x \frac{1}{\sqrt{1-x^2}} T_n(x)^2 = \begin{cases} \frac{1}{2}\pi & \text{if } n \neq 0 \\ \pi & \text{if } n = 0. \end{cases}$$

Condition (A.7) leads to the integral equation

$$\sum_{m=1}^{M_G} a_m J_m(kR) \int_{\alpha}^{\pi} \mathrm{d}x\, \omega\left(\frac{2x - (\pi + \alpha)}{\pi - \alpha}\right) \times T_j\left(\frac{2x - (\pi + \alpha)}{\pi - \alpha}\right) \sin x = 0 \qquad j = 1, 2, \ldots, N. \tag{A.9}$$

The integer N is determined by the number of unknown coefficients a_m.

To obtain the solution for the entire system the solutions obtained from (A.1) and (A.6) have to be joined smoothly along the chord which is common to the circle and the channel. This is done by the requirement

$$\begin{aligned} &\Psi_{ci}(0, y) = \Psi_{ch}(0, y) \\ &\frac{\partial \Psi_{ci}}{\partial x}(x, y)\bigg|_{x=0} = \frac{\partial \Psi_{ch}}{\partial x}(x, y)\bigg|_{x=0} \qquad \forall y \in [0, W]. \end{aligned} \tag{A.10}$$

Again, it is most efficient to expand both wavefunctions and there first derivatives with respect to an adequate set of orthogonal functions. An appropriate function is $\sin(\pi n y/L)$, $n = 1, 2, \ldots$, because then on the RHS of the resulting equations for the expansion coefficients in the sum over t (see (A.4)) all but one term vanish. The corresponding set of equations reads

$$\begin{aligned} &\sum_{m=1}^{M_G} a_m \frac{2}{\sqrt{L}} \int_0^L \mathrm{d}y \sin\left(\frac{\pi n}{L} y\right) \sin(m\varphi_d) J_m(kr_d) = (\delta_{rn} + T_{rn}) \frac{1}{\sqrt{|k_n|}} \\ &\sum_{m=1}^{M_G} a_m \frac{2}{\sqrt{L}} \int_0^L \mathrm{d}y \sin\left(\frac{\pi n}{L} y\right) \left(\sin(m\varphi_d) \frac{kd}{r_d} J_{m-1}(kr_d) \right. \\ &\qquad \left. - m[y \cos(m\varphi_d) + d \sin(m\varphi_d)] \frac{1}{r_d^2} J_m(kr_d) \right) \\ &\qquad = (\delta_{rn} - T_{rn}) \frac{k_n}{\mathrm{i}\sqrt{|k_n|}} \\ &\varphi_d = \tan^{-1}\left(\frac{y}{d}\right) \qquad r_d = \sqrt{d^2 + y^2} \qquad n = 1, 2, \ldots, L + M_C. \end{aligned} \tag{A.11}$$

After multiplying the first of these equations with $\sqrt{|k_n|}$, the second with $\mathrm{i}\sqrt{|k_n|}/k_n$ the unknown matrix elements T_{rs} can be eliminated by adding the resulting equations. Equation (A.9) provides N and (A.11), for a given incoming mode k_r, $(L + M_C)$ equations for the determination of the coefficients a_m in (A.8). These are all M_G unknowns so that

$$M_G = N + L + M_C. \tag{A.12}$$

The scattering matrix is obtained from one of the equations (A.12) by inserting the calculated values for a_m. For a given dimension L of the scattering matrix S, M_G and M_C have been varied and for each choice the accuracy has been checked in several ways:

(i) The resulting scattering matrix has to be symmetric, because the scattering system is invariant under time reversal.

(ii) The absolute value of the determinant of S has to equal 1, $|\det S| = 1$. We have chosen M_G and M_C such that $|\det S|$ deviates from 1 by less than 10^{-4}.

(iii) We have inserted the numerically obtained values of a_m into that equation derived from (A.11), which does not contain T_{rn} and required that it is fulfilled up to a correction of less than 10^{-6}.

References

[1] Jung C and Scholz H J 1987 *J. Phys. A: Math. Gen.* **20** 3607
[2] Tél T 1987 *Phys. Rev.* A **36** 1502

[3] Blümel R and Smilansky U 1990 *Phys. Rev. Lett.* **64** 241
[4] Sjöstrand J 1987 *Commun. Math. Phys.* **108** 391
[5] Gaspard P and Rice S A 1989 *J. Chem. Phys.* **90** 2225, 2242, 2255
[6] Ericson T 1960 *Phys. Rev. Lett.* **5** 430; 1963 *Ann. Phys.* **23** 390
[7] Wigner E 1951 *Ann. Phys.* **53** 36; 1952 *Ann. Phys.* **55** 7
[8] Bleher S, Ott E and Grebogi C 1989 *Phys. Rev. Lett.* **63** 919
[9] Troll G 1991 *Physica* **50D** 276
[10] Jung C 1986 *J. Phys. A: Math. Gen.* **19** 1345
[11] Doron E and Smilansky U 1991 *Proc. of the NATO 'Quantum Chaos' Advanced Study Workshop (Copenhagen)* to appear
[12] Balian R and Bloch C 1978 *Ann. Phys.* **69** 76
[13] Berry M V 1981 *Ann. Phys.* **131** 163
[14] Bunimovich L A 1979 *Commun. Math. Phys.* **65** 295
[15] Berry M V 1981 *Eur. J. Phys.* **2** 91
[16] Bogomolny E 1991 Private communication
[17] Doron E 1991 Private communication
[18] Doron E and Smilansky U 1992 Semiclassical quantization of chaotic billiards *Preprint W15-91/63/Sep-PH* Weizmann Institute
[19] Doron E, Smilansky U and Frenkel A 1991 *Physica* **50D** 36
[20] Levine E, Shtrikman S and Treves D 1988 *IEE Proceedings* **135H** 54
Levine E, Matzner H and Shtrikman S 1989 *Electromagnetics* **9** 451
[21] Berry M V 1985 *Proc. R. Soc.* A **400** 229
[22] Smilansky U 1989 *Proc. of the 1989 Les Houches Summer School on 'Chaos and Quantum Physics'*
[23] Troll G and Smilansky U 1989 *Physica* **35D** 34
[24] Blümel R and Smilansky U 1989 *Physica* **36D** 111
[25] Doron E and Smilansky U 1992 To be published
[26] Dyson F J 1962 *J. Math. Phys.* **3** 140